Protein structure and dynamics by NMR

Otten, Renee

Chapter 5

Comprehensive Determination of $^{3}J_{\mathrm{H^{N}H^{\alpha}}}$ for Unfolded Proteins Using $^{13}\mathrm{C}'$-Resolved Spin–Echo Difference Spectroscopy

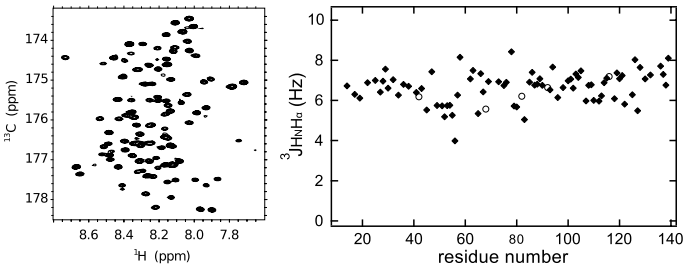

Renee Otten*, **Kathleen Wood*** **and Frans A. A. Mulder**

Groningen Biomolecular Sciences and Biotechnology Institute (GBB), University of Groningen, Nijenborgh 4, 9747 AG Groningen, The Netherlands

* both authors contributed equally to this work

Published in 2009 in *Journal of Biomolecular NMR*, **45** (4): 343 – 349

5.1 Abstract

An experiment is presented to determine $^3J_{H^NH^\alpha}$ coupling constants, with significant advantages for applications to unfolded proteins. The determination of coupling constants for the peptide chain using 1D ^{1}H, or 2D and 3D $^1H-^{15}N$ correlation spectroscopy is often hampered by extensive resonance overlap when dealing with flexible, disordered proteins. In the experiment detailed here, the overlap problem is largely circumvented by recording $^1H-^{13}C'$ correlation spectra, which demonstrate superior resolution for unfolded proteins. *J*-coupling constants are extracted from the peak intensities in a pair of 2D spin–echo difference experiments, affording rapid acquisition of the coupling data. In an application to the cytoplasmic domain of human neuroligin-3 (hNlg3*cyt*) data were obtained for 78 residues, compared to 54 coupling constants obtained from a 3D HNHA experiment. The coupling constants suggest that hNlg3*cyt* is intrinsically disordered, with little propensity for structure.

5.2 Introduction

Disordered proteins attract increasing attention, due in part to the fact that intrinsic disorder is prevalent in the proteomes of higher order organisms (Ward et al., 2004). In addition, it has been established that the disordered states of proteins are not mere featureless "random coils", but are characterized by secondary structure propensities of the polypeptide backbone, sometimes augmented with specific local interactions between side chains (Dill & Shortle, 1991; Shortle, 1996; Wirmer et al., 2005; Mittag & Forman-Kay, 2007). High-resolution determination of residual structure in these inherently flexible molecules is therefore necessary (Bartlett & Radford, 2009). NMR spectroscopy is undoubtedly the most appropriate technique to offer detailed insight into disordered states, being sensitive to the length and time scales characterizing the atomic structure (Wirmer et al., 2005; Bartlett & Radford, 2009; Eliezer, 2009; Mulder et al., 2009). In our analyses of intrinsically disordered proteins (IDPs) we have been interested in the measurement of scalar coupling constants to probe the local polypeptide backbone structure. To this end we have employed experiments that have been very successfully applied to folded proteins, and for which careful parameterization of three-bond coupling constants as a function of the backbone angle ϕ are available (Billeter et al., 1992; Vuister

& Bax, 1993; Case et al., 2000). For example, the most effectual and widely used coupling constants to define the backbone geometry, $^{3}J_{\mathrm{H^{N}H^{\alpha}}}$, can be determined efficiently from a pair of 2D spin–echo difference measurements, obtained as HMQC (Ponstingl & Otting, 1998) or HSQC (Petit et al., 2002) variants, recorded on ^{15}N-labeled proteins. 2D $^{1}\mathrm{H}-^{15}\mathrm{N}$ correlation spectra of unfolded proteins are, however, severely compromised by resonance overlap, thereby limiting the number of probes available for conformational analysis. Since 3D experiments (Vuister & Bax, 1993; Kuboniwa et al., 1994) to measure $^{3}J_{\mathrm{H^{N}H^{\alpha}}}$ include the 2D $^{1}\mathrm{H}-^{15}\mathrm{N}$ correlations as "diagonal peaks", overlap in the 2D spectrum comparatively reduces the utility of 3D spectroscopy for the measurement of $^{3}J_{\mathrm{H^{N}H^{\alpha}}}$ in unfolded proteins. In an elegant approach, Lendel & Damberg (2009) very recently showed that improved resolution can be obtained by effectively removing the homonuclear coupling from the proton line width in a 3D *J*-resolved $^{1}\mathrm{H}-^{15}\mathrm{N}$ correlation spectrum, and were thereby able to achieve a near-complete analysis of the coupling constants for the natively disordered protein α-synuclein. In this paper we present an alternative approach to achieve excellent spectral resolution, which is based on 2D spectroscopy.

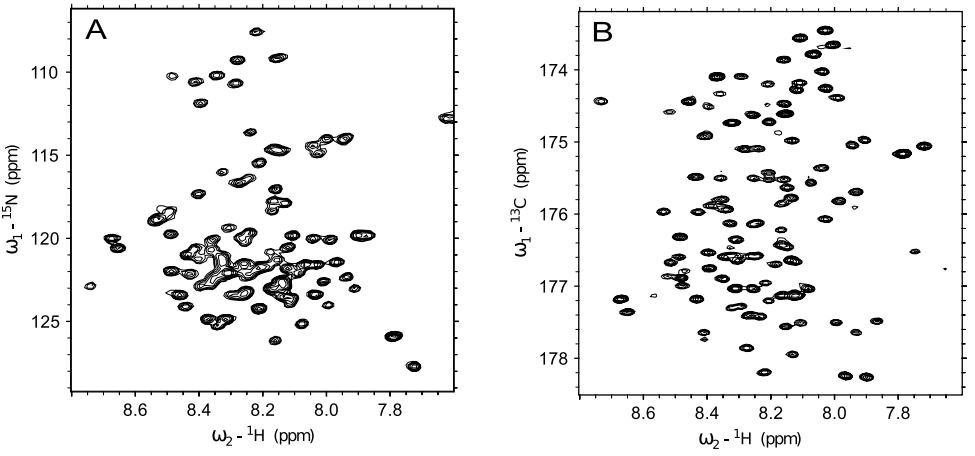

Figure 5.1. 2D $^{1}\mathrm{H}-^{15}\mathrm{N}$ HSQC (panel A) and $^{1}\mathrm{H}-^{13}\mathrm{C}'$ H(N)CO (panel B) correlation spectra for the 139 amino acid construct of the intrinsically disordered protein domain hNlg3*cyt*.

We show here that a much more complete set of $^{3}J_{\mathrm{H^{N}H^{\alpha}}}$ coupling constants can be obtained for uniformly (^{15}N,^{13}C)-labeled proteins by recording $^{13}\mathrm{C}'$, rather than ^{15}N, chemical shift modulation in the indirectly detected domain. The rationale for this strategy was derived from a comparison of 2D $^{1}\mathrm{H}-^{15}\mathrm{N}$ and $^{1}\mathrm{H}-^{13}\mathrm{C}'$ corre-

lation spectra (*viz.* Figure 5.1) for the cytoplasmic domain of human neuroligin-3 (hNlg3*cyt*), obtained with gradient-sensitivity enhanced HSQC (Kay et al., 1992b) and HNCO (Yang & Kay, 1999a) experiments, respectively. Both experiments were recorded with 100 complex time points in the indirect dimension, and processed identically. Figure 5.1 clearly demonstrates the improvement in resolution that is obtained in the $^1H-^{13}C'$ spectrum of the unfolded protein, compared to $^1H-^{15}N$ correlation spectroscopy. In addition to the higher apparent spread of the signals in the $^1H-^{13}C'$ spectrum, the $^{13}C'$ line widths (measured at 14.1 T) are also significantly smaller. For example, in the case of hNlg3*cyt*, the natural line widths measured in $^1H-^{13}C'$ and $^1H-^{15}N$ spectra were 5.6 and 16.2 Hz, respectively.

5.3 Results and Discussion

With the high resolution of $^1H-^{13}C'$ correlation spectroscopy in mind we developed a novel pulse sequence to measure $^3J_{H^NH^\alpha}$ for uniformly ^{15}N,^{13}C-enriched proteins, which is shown in Figure 5.2. The scheme is a combination of HNCO triple resonance spectroscopy (Yang & Kay, 1999a) and HMQC-based spin–echo difference $^3J_{H^NH^\alpha}$ experiments (Ponstingl & Otting, 1998): through successive INEPT transfer steps the starting amide polarization is transferred to $^{13}C'$ for chemical shift encoding. The sequence of events up to point *a* can be described as $H_Z \rightarrow 2N_ZC'_Z$, and, after a 90° $^{13}C'$ pulse is followed by carbonyl carbon chemical shift encoding. Subsequently, at point *b* in the sequence, evolution of the anti-phase term $-2N_YC'_Z$ takes place under the one-bond $^{15}N-^{13}C'$ and $^{15}N-^1H$ coupling Hamiltonians simultaneously. After a delay $\kappa = 1/(2 \times {}^1J_{NH})$ the density operator is proportional to $4H_ZN_XC'_Z \cdot \cos(\pi J_{NC'}\kappa) + 2H_ZN_Y \cdot \sin(\pi J_{NC'}\kappa)$. A 90° ^1H pulse transforms this into $-4H_YN_XC'_Z \cdot \cos(\pi J_{NC'}\kappa) - 2H_YN_Y \cdot \sin(\pi J_{NC'}\kappa)$, which interrupts any further evolution under the proton-nitrogen coupling, while allowing now for the simultaneous evolution under the one-bond $^{13}C'-^{15}N$ and three-bond $^1H^N-^1H^\alpha$ coupling Hamiltonians. At point *c* in the sequence the refocusing due to $^1J_{NC'}$ is complete. Subsequently, after the final 90° ^{15}N pulse, evolution under the mutual scalar coupling for a period κ also completely refocuses the nitrogen-proton anti-phase terms. A non-selective 180° proton pulse in the middle of the multiple-quantum (MQ) evolution period ensures that ^1H chemical shift evolution is fully refocused. In total, evolution due to the $^3J_{H^NH^\alpha}$ coupling equals 2T at that point. After the last 90° ^1H pulse the only terms present are now

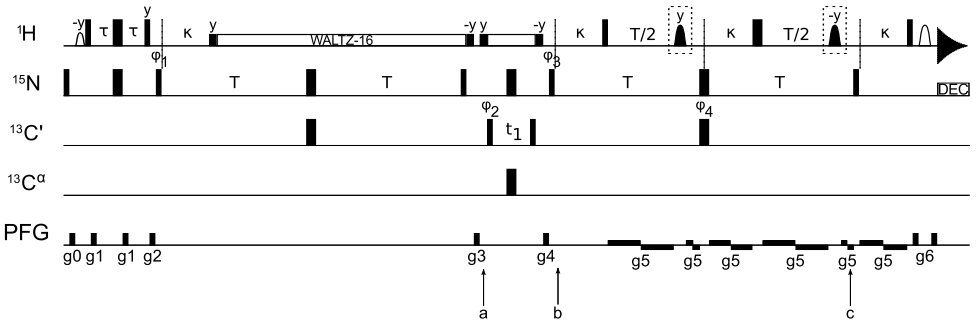

Figure 5.2. Pulse sequence of the $^{13}C'$-resolved spin–echo difference experiment to measure $^{3}J_{H^{N}H^{\alpha}}$. Two versions of the experiment are executed, one with the boxed inversion pulses present (A) and one without (B). Narrow (wide) filled bars indicate 90° (180°) RF pulses applied along the x-axis, unless otherwise indicated. The ^{1}H carrier is centered at the water resonance (4.76 ppm) and proton pulses are applied with a field strength of $\omega_1/2\pi$ = 37.3 kHz. Proton decoupling is achieved using a WALTZ-16 decoupling scheme with $\omega_1/2\pi$ = 5.0 kHz. The water flip-back pulse at the beginning of the sequence has an EBURP-1 profile (Geen & Freeman, 1991) ($\omega_1/2\pi$ = 715 Hz, 5.12 ms duration). The filled dome shaped proton pulses are used for the selective inversion of the $^{1}H^{\alpha}$ region and have an IBURP-2 profile ($\omega_1/2\pi$ = 1.75 kHz, 2.9 ms duration). The open dome shaped proton pulse has a REBURP profile and inverts only the amide region ($\omega_1/2\pi$ = 1.55 kHz, 4.01 ms duration) through phase-modulation. The ^{15}N carrier is centered at 117 ppm and nitrogen pulses are applied with a field strength of $\omega_1/2\pi$ = 6.0 kHz. Rectangular 90° (180°) ^{13}C pulses are applied with a field of $\omega_1/2\pi = \Delta/\sqrt{15}$ ($\Delta/\sqrt{3}$), where Δ is the difference (in Hz) between $^{13}C^{\alpha}$ (57 ppm) and $^{13}C'$ (176 ppm). Decoupling during acquisition is done using GARP-1, with $\omega_1/2\pi$ = 1.25 kHz. Values of the delays are τ = 2.3 ms, κ = 5.4 ms, T = 16.67 ms. Gradient strengths in G/cm (length in ms) are g_0 = 8.0 (0.5), g_1 = 5.0 (0.5), g_2 = 15.0 (2.0), g_3 = 20.0 (0.75), g_4 = 15.0 (2.0), g_5 = 1.0 (variable), g_6 = 21.0 (0.1). The phase cycling is ϕ_1 = x; ϕ_2 = [x,–x]; ϕ_3 = [x,x,–x,–x]; ϕ_4 = [x,–x]; ϕ_{rec} = [x,–x,–x,x]. Quadrature detection in F_1 is obtained by incrementing ϕ_2, according to the States-TPPI protocol.

$H_X \cdot \cos(\pi J_{H^N H^\alpha} 2T) - 2H_Z H_Y^\alpha \cdot \sin(\pi J_{H^N H^\alpha} 2T)$. Only the in-phase term survives the subsequent echo period, which is comprised of an amide proton-selective REBURP refocusing pulse (Geen & Freeman, 1991), combined with a gradient echo. This short additional element is also necessary to suppress any small amount of water magnetization that is not returned to the +Z axis by the last 90° ^{1}H pulse in the sequence. Fourier transformation leads to an absorptive signal at the amide proton chemical shift, with its intensity encoding the three-bond $^{1}H^{N} - {}^{1}H^{\alpha}$ coupling constant. In order to quantify the $^{3}J_{H^{N}H^{\alpha}}$ coupling constants a reference measurement is performed, during which selective inversion of $^{1}H^{\alpha}$ is achieved

at time points T/2 (= 1/(4 x $^1J_{NC'}$) and 3T/2 (= 3/(4 x $^1J_{NC'}$), thereby effectively refocusing the coupling (these pulses are shown as boxed filled domes in Figure 5.2). For this purpose, IBURP-2 pulses (Geen & Freeman, 1991) were employed, which effect a rapid inversion during the central segment of the pulse. Practically, two experiments are recorded: one with the selective $^1H^\alpha$ pulses (I_A) and one without (I_B). Residue-specific values for the three-bond coupling constants are calculated from the intensity ratios of the resulting spectral signals as

$$^3J_{H^NH^\alpha} = (2\pi T)^{-1} \arccos(I_B/I_A)$$

A few further aspects of the experiment are worth mentioning at this point. First, during the final part of the pulse sequence, no sensitivity losses incur from the refocusing of $-2N_YC'_Z$ during the 2T period of 33 ms. The MQ evolution period nicely combines the refocusing period with the period that is required for the three-bond proton-proton coupling evolution, since these two processes require approximately the same amount of time.

Second, ^{1}H composite pulse decoupling is applied during $^{13}C'$ evolution, since three-bond couplings to β-protons (2–6 Hz) would otherwise contribute to unresolved line broadening. Under these conditions narrow lines are observed for $^{13}C'$, due to the absence of strong relaxation mechanisms: the dominant source of relaxation, even at moderate static magnetic field strength, is the chemical shift anisotropy (CSA), which is modest at 14.1 T. Since protons are far removed from the carbonyl carbon atom, dipolar relaxation contributions are small. For unfolded proteins a three-fold reduction in the line widths was observed by recording $^{13}C'$ rather than ^{15}N-resolved spectra (see above), and this advantage also extends to folded proteins: for calbindin D_{9k} the average carbonyl line width is 6.4 Hz, compared with 20.0 Hz for nitrogen. In addition, the high spectral dispersion displayed by $^{13}C'$ arises from the fact that the carbonyl chemical shift is influenced by the neighboring residue types to both sides (Wishart et al., 1995a; Yao et al., 1997; Wang & Jardetzky, 2002). The favorable relaxation properties and sequence-specific shielding contributions together ensure the high inherent resolution for $^1H-^{13}C'$ correlation spectroscopy displayed by disordered proteins.

Third, a water flip-back strategy is used to avoid the transfer of water saturation to the solvent-exposed, exchangeable amide protons. Since all amides in the unfolded state are solvent-exposed, care has to be taken to control the state of water

throughout the pulse sequence. Failure to establish that the water polarization is very similar in each of the two spin–echo difference experiments could lead to significant systematic errors. A three-pronged approach was taken here: (1) Since radiation damping can rapidly cause the large out-of-equilibrium water polarization to align with the external magnetic field we have limited the time during which it is not aligned along the +Z axis; (2) During the chemical shift evolution period where the water polarization is along –Z, weak gradients are employed to rapidly dephase any magnetization that rotates away from the –Z axis; (3) When the magnetization is in the transverse plane it is kept locked by a strong ($\omega_1/2\pi \sim$5 kHz) rotating transverse field, which is simultaneously used for composite pulse ^{1}H decoupling. Residual water suppression after the final 90° ^{1}H pulse is achieved by a selective $^1H^N$ REBURP refocusing pulse (Geen & Freeman, 1991), bracketed by gradients, akin to the WATERGATE procedure (Piotto et al., 1992). Rather than judging the effectiveness of the water flip-back procedure from the degree of water suppression, an optional 90° ^{1}H pulse was included at the end of the pulse sequence to query the longitudinal water polarization prior to acquisition. This was done, by comparing the signal intensity with that obtained after a single 90° ^{1}H pulse. To avoid receiver overflow, the signal was moderated, by placing a 6 dB attenuator between the preamplifier and the observation receiver (i.e., prior to signal digitization). In this way it was established that the flip-back strategy was effective to 95% or better. More importantly, the water state was no different in the experiments that do or do not contain selective $^1H^\alpha$ decoupling pulses. We found that this procedure yielded more reliable estimates of the water signal magnitude, than using a short tapping pulse.

To benchmark the experimental procedure, the new pulse sequence was first applied to the small folded protein calbindin D_{9k}, and measured $^3J_{H^NH^\alpha}$ values were compared with coupling constants derived from a 3D HNHA experiment (Vuister & Bax, 1993). The 3D data set was recorded using 47 x 62 complex data points for the proton and nitrogen domain, corresponding to maximum evolution times of 5.9 and 31.9 ms, respectively. Linear prediction was used in both indirect domains, followed by strongly apodizing window functions. The coupling constants extracted using this procedure were the same as those obtained without linear prediction. The total acquisition time was 30 h. For the 2D measurement 256 complex points were acquired in the $^{13}C'$ domain, using a maximum evolution time of 170.7 ms. A pair of experiments (once with and once without modulation due to the three-bond coupling) was recorded in 6 h, and this procedure was

repeated four times, in an interleaved fashion, to ensure that any changes would affect both experiments equally, and the data was subsequently added together.

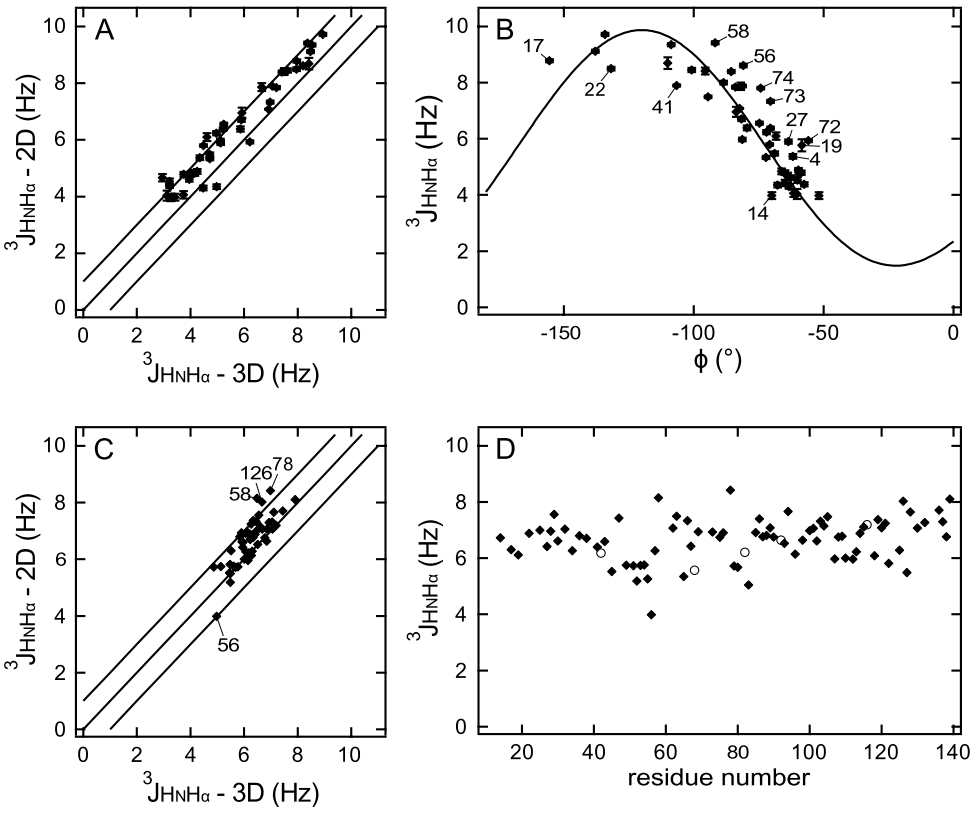

Figure 5.3. **(a)** Comparison of experimental $^3J_{H^NH^\alpha}$ coupling constants for the small folded protein calbindin D_{9k}, obtained using 2D $^1H-^{13}C'$ spin–echo difference and 3D HNHA experiments. Error bars on the 3D data set are similar to the size of the symbols, and are not shown for clarity. **(b)** Comparison of the experimental 2D $^1H-^{13}C'$ spin–echo difference derived $^3J_{H^NH^\alpha}$ coupling constants for calbindin D_{9k} with those calculated from the 1.6 Å X-ray crystal structure (Svensson et al., 1992) 4ICB, using the Karplus parametrization by Vuister & Bax (1993). **(c)** Comparison of experimental $^3J_{H^NH^\alpha}$ coupling constants for the intrinsically disordered protein domain hNlg3*cyt*, obtained using 2D $^1H-^{13}C'$ spin–echo difference and 3D HNHA experiments. Error bars are of similar size as the sample points. **(d)** $^3J_{H^NH^\alpha}$ coupling constants for the intrinsically disordered protein domain hNlg3*cyt*, obtained with the new pulse sequence. Error bars are smaller than the size of the symbol for most data points. Empty circles show 3D HNHA-derived coupling constants for five additional residues, which give rise to overlapped cross-peaks in the 2D $^1H-^{13}C'$, but not in the 2D $^1H-^{15}N$ spectrum.

As Figure 5.3a shows, there is excellent agreement between the coupling constants for this protein, derived from 2D and 3D measurements, except for the presence of a systematic difference between the two data sets. Coupling constants obtained for ten residues for which the selective pulses do not perfectly effect the desired inversion of $^1H^\alpha$ magnetization, or completely refocus the $^1H^N$ region were excluded from the analysis, and Figure 5.3a. For example, $^3J_{H^NH^\alpha}$ values for Leu31 and Phe63 appeared seriously underestimated in the 2D measurement. This outcome was anticipated, as the $^1H^\alpha$ chemical shifts for Leu31 and Phe63 are 2.37 and 3.32 ppm, respectively, and fall outside the region for proper inversion. Although differential relaxation of the in-phase and anti-phase terms in the 3D HNHA scalar coupling measurement may lead to the systematic underestimation of the true J values for larger proteins (Harbison, 1993; Kuboniwa et al., 1994; Vögeli et al., 2007), the short rotational correlation time for calbindin D_{9k} (τ_c = 4.2 ns) suggests that a correction for differential relaxation would amount to underestimations of the true J couplings by approximately 5% (Kuboniwa et al., 1994). Even after making this correction it appears that the values from the 3D HNHA experiment underestimate the scalar coupling values by about 0.5 Hz. Interestingly, Wang & Bax (1996) required a similar systematic increase of 3D HNHA-derived relaxation-corrected $^3J_{H^NH^\alpha}$ values for human ubiquitin (0.4 Hz) to obtain satisfactory agreement with values obtained using 2D J-modulated CT-HMQC spectra and HNCA[HA]-E.COSY experiments. It therefore appears that the J couplings measured with the proposed 2D spin–echo difference scheme are robust, even for small folded proteins.

The experimental coupling constants were compared with those calculated from a 1.6 Å X-ray crystal structure 4ICB (Svensson et al., 1992), using the Karplus parametrization by Vuister & Bax (1993). The agreement with the 2D spin–echo difference derived coupling constants is very good, although there are a number of residues for which the coupling constants are further removed from the calculated curve than would be expected from the quality of the data. There exist two explanations for these differences. The first reason is that values for $^3J_{H^NH^\alpha}$ calculated from a single static structure cannot be expected to faithfully represent experimental data in the case of dynamics. Residues that are known to be flexible from NMR relaxation studies (Kördel et al., 1992) indeed show poor agreement. For example, residues belonging to the termini (Glu4, Lys72–Ser74) and the linker region (Lys41) yield values between 6 and 8 Hz, indicative of averaging, and are more than 1 Hz removed from the values calculated from a static structure. Second, a number of

further deviations appear to be the result of true differences between the structures in the crystal lattice and in solution. Calbindin D_{9k} contains two loops, which coordinate a calcium ion each, providing backbone as well as side chain oxygen ligands. The first loop comprises Ala14–Glu27, and the second extends from Asp54 to Glu65. It is observed that data for residues of the four helices nicely fit to the Karplus relation, whereas the experimentally determined J couplings for all other residues that deviate by more than 1 Hz from calculation map to the two calcium binding loops. These are indicated in Figure 5.3b. It appears that backbone angles in the loop regions differ by up to 10° between the crystalline and solution states. This assertion is confirmed by ${}^3J_{C'C'}$ couplings, which report on the same dihedral angle (data not shown).

Once the methodology was validated, we applied the experiment to the disordered protein domain hNlg3*cyt*. In a previous study the structural nature of this domain was studied by a host of biophysical methods, including small-angle X-ray scattering, CD spectroscopy and NMR spectroscopy (Paz et al., 2008). The main conclusion of that work was that hNlg3*cyt* belongs to the family of intrinsically disordered proteins (IDPs), also referred to as natively unfolded proteins. Since no NMR assignments were available at the time of that study, the experimental data were used to derive an overall picture of the protein's physical state. Meanwhile we have obtained near-complete backbone resonance assignments of the protein, such that a site-specific analysis of order and disorder in the sequence can be undertaken. Because scalar coupling constants are very sensitive to the local order of the peptide bond, they would serve as excellent probes to detect any residual structural propensity along the polypeptide chain.

Using the 3D HNHA experiment, a data set of 46 x 62 complex data points was collected for the proton and nitrogen domain, corresponding to maximum evolution times of 5.7 and 31.9 ms, respectively. The total measuring time was 30 h. Due to extensive overlap we were only able to obtain 54 ${}^3J_{H^N H^\alpha}$ values for hNlg3*cyt* from this data set. Therefore the pulse sequence of Figure 5.2 was employed, using 128 complex data points for the ${}^{13}C'$ dimension, with a maximum evolution time of 160.0 ms. The experiments with and without ${}^1H^\alpha$ decoupling were repeated four times. The total measuring time was 30 h. Making use of the 2D ${}^1H-{}^{13}C$ correlation spectra, the number of probes amenable to analysis increased to 78, out of 105 possible (139-residue long sequence, with 10 amino acids in the poly-histidine tag, 16 proline and 8 glycine residues). Of note, for unfolded proteins the clear separation of the narrow ${}^1H^\alpha$ (4.0–4.8 ppm) and ${}^1H^N$

(7.9–8.7 ppm) chemical shift ranges does not hinder the coupling measurement as it does for folded proteins (see above), and no data needed to be excluded from further analysis. A single outlier was obtained (residue 56), but the reason for this discrepancy is currently unknown.

The $^{3}J_{\mathrm{H^N H^\alpha}}$ values measured for hNlg3*cyt* by 3D HNHA and 2D spin–echo difference spectroscopy are compared in Figure 5.3c. Since the inter-proton dipolar correlation times in unfolded proteins are much smaller than those of folded proteins, it is unlikely that the effects due to differential relaxation need to be taken into account (Harbison, 1993; Kuboniwa et al., 1994; Rexroth et al., 1995). However, a small systematic difference of about 0.4 Hz is still observed, as was the case for calbindin D_{9k}. Such a systematic difference has previously been attributed to an underestimation of the coupling constants using the 3D HNHA experiment, suggesting that the values derived with the new experiment are reliable. In addition, since the 2D spin–echo difference-derived coupling constants agree well with the three-dimensional molecular structure for calbindin D_{9k}, $^{3}J_{\mathrm{H^N H^\alpha}}$ values for unfolded proteins can be used as reliable probes of polypeptide conformation.

A plot of the measured $^{3}J_{\mathrm{H^N H^\alpha}}$ for hNlg3*cyt* as a function of residue number is shown in Figure 5.3d. The average value of ca. 7 Hz is similar to values obtained for flexible peptides and other disordered peptides, corroborating earlier results (Paz et al., 2008). However, a few regions deviate from this trend, showing significantly lower values. The interpretation of this result is that conformations with values for the angle ϕ toward –60° are increasingly being populated. Importantly, from $^{3}J_{\mathrm{H^N H^\alpha}}$ values alone it is not possible to say whether these include canonical α-helical or polyproline type II (PPII) structures. This will await further investigation, and an analysis of additional experimental data is beyond the scope of this work, and will be presented elsewhere.

In summary, an experiment is presented to measure $^{3}J_{\mathrm{H^N H^\alpha}}$, employing $^{13}\mathrm{C}'$- instead of ^{15}N-resolved experiments. The sizeable gain in the number of probes that become available for unfolded proteins suggests that the proposed experiment serves as an important complement to characterize the structure and dynamics of disordered states of proteins.

5.4 Acknowledgment

We thank Dr. Aviv Paz and Prof. Joel Sussman (Weizmann Institute, Rehovot, Israel) for the sample used in this study. K.W. acknowledges a post-doctoral fellowship from the European Molecular Biology Organization (EMBO). This work was supported by a VIDI grant to F.A.A.M. from The Netherlands Organization for Scientific Research (NWO).